PHYSICAL REVIEW D **95,** 115010 (2017)

Lepton-number-violating searches for muon to positron conversion

Jeffrey M. Berryman,[1] André de Gouvêa,[1] Kevin J. Kelly,[1] and Andrew Kobach[2]
[1]*Northwestern University, Department of Physics & Astronomy, 2145 Sheridan Road, Evanston, Illinois 60208, USA*
[2]*Department of Physics, University of California, San Diego, La Jolla, California 92093, USA*
(Received 12 December 2016; published 8 June 2017)

There is no guarantee that the violation of the lepton number, assuming it exists, will primarily manifest itself in neutrinoless double beta decay ($0\nu\beta\beta$). Lepton-number violation and lepton-flavor violation may be related, and much-needed information regarding the physics that violates the lepton number can be learned by exploring observables that violate lepton flavors other than the electron flavor. One of the most promising observables is the $\mu^- \to e^+$ conversion, which can be explored by experiments that are specifically designed to search for the $\mu^- \to e^-$ conversion. We survey lepton-number violating dimension-five, -seven, and -nine effective operators in the standard model and discuss the relationships between Majorana neutrino masses and the rates for $0\nu\beta\beta$ and the $\mu^- \to e^+$ conversion. While $0\nu\beta\beta$ has the greatest sensitivity to new ultraviolet energy scales, its rate might be suppressed by the new physics relationship to lepton flavor, and the $\mu^- \to e^+$ conversion offers a complementary probe of lepton-number-violating physics.

DOI: 10.1103/PhysRevD.95.115010

I. INTRODUCTION

Neutrino flavor oscillations imply that at least two neutrinos have nonzero masses and that there is nontrivial mixing in the lepton sector. The mechanism behind nonzero neutrino masses is currently unknown, and a definitive resolution of the neutrino mass puzzle will require input from a variety of probes of fundamental physics, including neutrino oscillation experiments, searches for lepton-number and baryon-number violation, precision measurements of charged-lepton properties and rare processes, and high-energy collider experiments.

Tests of the validity of lepton-number conservation are among the most valuable sources of information when it comes to the neutrino mass puzzle (see, for example, Ref. [1], for an overview). They provide unique information on the nature of the neutrino, i.e., whether it is a Dirac or a Majorana fermion. Speculations on the origin of neutrino masses, in turn, differ dramatically depending on the nature of the neutrino. While searches for neutrinoless double beta decay ($0\nu\beta\beta$) are, by far, the most powerful available probes of lepton-number violation (see Ref. [2] for a thorough overview), the pursuit of other lepton-number-violating (LNV) observables is of the highest importance.

Searches for charged-lepton-flavor violation are also potentially powerful probes of the origin of neutrino masses (see, for example, Refs. [1,3], for an overview). Among the different charged-lepton-flavor-violating processes, powerful new searches for the $\mu^- \to e^-$ conversion in nuclei are currently being developed [4–6]. These are expected to improve on the current sensitivity to the $\mu^- \to e^-$ conversion rate by at least 4 orders of magnitude in less than a decade.

Experiments sensitive to the $\mu^- \to e^-$ conversion in nuclei may also serve as laboratories to search for the LNV $\mu^- \to e^+$ conversion in nuclei (see, for example, Refs. [6,7]). The current upper bound on this conversion rate, normalized to the capture rate, is 1.7×10^{-12} for the transition between titanium and the ground state of calcium, obtained by the SINDRUM II Collaboration [8]. Significant improvement is expected from at least a subset of the next-generation $\mu^- \to e^-$ conversion experiments.

Here, we estimate the capabilities of next-generation $\mu^- \to e^-$ conversion experiments to discover or constrain $\mu^- \to e^+$ conversion in nuclei. We also explore how these results can relate to searches for $0\nu\beta\beta$ and nonzero Majorana neutrino masses. We make use of the standard model (SM) effective operator approach—introduced in Ref. [9] and explored in, for example, Refs. [10–16]—in order to gauge the impact of these future measurements on a large variety of neutrino mass models. This approach is powerful and allows one to relate different LNV observables, including nonzero neutrino masses. Extended versions of this approach have been successfully pursued in order to relate, assuming grand unification is realized in nature, lepton-number and baryon-number violating observables [17]. For other comparisons of $\mu^- \to e^+$ conversion in nuclei to different LNV observables see, for example, Refs. [2,18,19]. Reference [19], which appeared in the literature shortly before this work, asks some of the questions we address here, but our approaches are somewhat complementary. More concretely, we analyze LNV phenomena using a different set of effective operators, as will be explained below.

This manuscript is organized as follows. In Sec. II, we estimate the sensitivity of different next-generation $\mu^- \to e^-$ conversion experiments to the $\mu^- \to e^+$ conversion in nuclei. In Sec. III, we review the effective operator approach and identify the operators of interest. We also review how the mass scale of the different effective operators can be related to the observed neutrino masses.

In Sec. IV, we discuss a few concrete examples of how we estimate the rates for the LNV processes of interest, and in Sec. V, we present and discuss our results. We present some concluding thoughts in Sec. VI. The Appendix contains a sample ultraviolet-complete scenario that can be described using the formalism discussed here.

II. SENSITIVITIES OF NEXT-GENERATION EXPERIMENTS

The SINDRUM II experiment at the Paul Scherrer Institute (PSI) was designed to investigate the $\mu^- \to e^-$ conversion in nuclei. The most recent result places a limit on the $\mu^- \to e^-$ conversion in gold [20],

$$R^{\mathrm{Au}}_{\mu^- e^-} \equiv \frac{\Gamma(\mu^- + \mathrm{Au} \to e^- + \mathrm{Au})}{\Gamma(\mu^- + \mathrm{Au} \to \nu_\mu + \mathrm{Pt})} < 7 \times 10^{-13} \quad (90\%\ \mathrm{C.L.}). \tag{2.1}$$

Nearly 10 years earlier, the SINDRUM II Collaboration also set a limit on the $\mu^- \to e^+$ conversion in titanium [8],

$$R^{\mathrm{Ti}}_{\mu^- e^+} \equiv \frac{\Gamma(\mu^- + \mathrm{Ti} \to e^+ + \mathrm{Ca})}{\Gamma(\mu^- + \mathrm{Ti} \to \nu_\mu + \mathrm{Sc})} < \begin{cases} 1.7 \times 10^{-12}\ (\mathrm{GS},\ 90\%\ \mathrm{C.L.}) \\ 3.6 \times 10^{-11}\ (\mathrm{GDR},\ 90\%\ \mathrm{C.L.}) \end{cases}, \tag{2.2}$$

where the top limit assumes coherent scattering to the ground state (GS) of calcium, while the bottom limit assumes a transition to a giant dipole resonance (GDR) state. The GS limit remains the strongest on any $\mu^- \to e^+$ conversion process to date. Next-generation experiments, however, are expected to improve upon it by several orders of magnitude.

The next generation of $\mu^- \to e^-$ conversion experiments includes Mu2e [6] at Fermilab in the United States and DeeMe [5] and COMET [4] (and its upgrade, PRISM [21]) at J-PARC in Japan. Mu2e and COMET/PRISM are schematically similar to SINDRUM II: a proton beam impinges upon a pion production target, and the muons produced in the pion decays are directed onto an aluminum stopping target. DeeMe is similar to these, except the pion production, muon production, and muon capture all take place in the same SiC target. The muons form bound states with the atomic nuclei, at which point one of the following happens: (i) the muons decay in orbit (DIO); (ii) they are captured by the nucleus, and a neutrino is produced; or (iii) they interact with the nucleus in a way not prescribed by the SM. DIO is one of the largest backgrounds at these experiments; the end point of the DIO electron spectrum coincides with the energy of the electron produced in $\mu^- \to e^-$ conversion. The spectrum of DIO electrons is calculable, however, and any unaccounted-for electrons in the region $E_e \sim m_\mu$ would constitute a signal. These experiments anticipate the following sensitivities [$R^{\mathrm{SiC}}_{\mu^- e^-}$ and $R^{\mathrm{Al}}_{\mu^- e^-}$ are defined analogously to Eq. (2.1)]:

$$\begin{aligned} \text{DeeMe:}\ & R^{\mathrm{SiC}}_{\mu^- e^-} > 5 \times 10^{-14}\ (90\%\ \mathrm{C.L.}), \\ \text{Mu2e:}\ & R^{\mathrm{Al}}_{\mu^- e^-} > 6.6 \times 10^{-17}\ (90\%\ \mathrm{C.L.}), \\ \text{COMET Phase-I:}\ & R^{\mathrm{Al}}_{\mu^- e^-} > 7.2 \times 10^{-15}\ (90\%\ \mathrm{C.L.}), \\ \text{COMET Phase-II:}\ & R^{\mathrm{Al}}_{\mu^- e^-} > 6 \times 10^{-17}\ (90\%\ \mathrm{C.L.}), \\ \text{PRISM:}\ & R^{\mathrm{Al}}_{\mu^- e^-} > 5 \times 10^{-19}\ (90\%\ \mathrm{C.L.}). \end{aligned}$$

Here we qualitatively estimate the sensitivities of these experiments to $\mu^- \to e^+$ conversion. At DeeMe, COMET Phase-II, and PRISM, the electrons ejected from the stopping target are transported away from the target to the spectrometer via magnetic fields. This helps to reject background events, but also means that, naively, any produced positrons will be "swept away" and not detected, rendering $\mu^- \to e^+$ conversion searches significantly more challenging and potentially unfeasible. We are therefore not able to infer a sensitivity for these experiments. Mu2e and COMET Phase-I, however, are a different story. The aluminum stopping targets are immersed in an external magnetic field, and the energies of emitted electrons are measured by determining their trajectories after they escape the stopping target. These experiments can then directly determine if an emitted lepton is an electron or a positron. This is precisely how limits on $R_{\mu^- e^+}$ were determined at SINDRUM II. We estimate the sensitivities of these experiments to $\mu^- \to e^+$ conversion as follows. In Ref. [22], the SINDRUM II Collaboration set limits on $R^{\mathrm{Ti}}_{\mu^- e^-}$ and $R^{\mathrm{Ti}}_{\mu^- e^+}$ (assuming transitions to the ground state of calcium) for the same experimental run,

$$\begin{aligned} R^{\mathrm{Ti}}_{\mu^- e^-} &< 4.3 \times 10^{-12}\ (90\%\ \mathrm{C.L.}), \\ R^{\mathrm{Ti}}_{\mu^- e^+} &< 4.3 \times 10^{-12}\ (90\%\ \mathrm{C.L.}). \end{aligned}$$

(That these two bounds are identical is a numerical accident.) Since these two limits are quite comparable to each other, we assume the improvements in the sensitivities to the $\mu^- \to e^-$ conversion and the $\mu^- \to e^+$ conversion scale commensurately and estimate that next-generation experiments will be sensitive to $\mu^- \to e^+$ rates greater than the following:

$$\begin{aligned} \text{Mu2e:}\ & R^{\mathrm{Al}}_{\mu^- e^+} \gtrsim 10^{-16}, \\ \text{COMET Phase-I:}\ & R^{\mathrm{Al}}_{\mu^- e^+} \gtrsim 10^{-14}. \end{aligned}$$

We emphasize that these are crude estimates. Detailed experimental analyses of the sensitivities of these experiments to the $\mu^- \to e^+$ conversion do not exist in the literature, and a realistic estimate can only be made in association with the existing experimental collaboration. We echo the sentiment recently expressed by the authors of Ref. [19], that such analyses should be pursued as they can potentially play a significant role in the study of LNV phenomena.

TABLE I. The dimension-five operator featured in this analysis. Naming convention follows from Refs. [11,15]. Parentheses denote fields that have their $SU(2)_L$ indices contracted to form a singlet. While not explicitly indicated, three generations of all fermions are contained in each operator. In the third column, Λ is the scale required to produce a neutrino mass in the range 0.05–0.5 eV, with lower Λ corresponding to higher neutrino mass. Analytic estimates of $T_{0\nu\beta\beta}$ and $R_{\mu^-e^+}$ are also listed, along with numerical estimates, assuming the operator in question is responsible for the observable neutrino masses. See text for details.

$\mathcal{O}$	Operator	Λ [TeV]	$T_{0\nu\beta\beta}$ $R_{\mu^-e^+}$
$\mathcal{O}_1$	$(LH)(LH)$	$6\times10^{10-11}$	$\ln(2)(\frac{\sqrt{2}}{G_F})^4(q^2)^2\frac{1}{v^4}\frac{\Lambda^2}{Q^{11}}\sim10^{25}$–$10^{27}$ yr $(\frac{G_F}{\sqrt{2}})^2(\frac{1}{q^2})^2\frac{v^4Q^6}{\Lambda^2}\sim10^{-38}$–$10^{-36}$

III. EFFECTIVE OPERATOR APPROACH

The SM Lagrangian can be augmented by operators with mass dimension $d>4$ that are constructed from SM matter fields (Q, u^c, d^c, L, e^c), Higgs bosons (H), field strength tensors ($G_{\mu\nu}$, $W_{\mu\nu}$, $B_{\mu\nu}$), and covariant derivatives (D_μ) (and their complex conjugates) and that respect both gauge and Lorentz invariance. These operators, however, need not respect the global symmetries of the baryon number and the lepton number. LNV phenomena, including $0\nu\beta\beta$ and neutrino Majorana masses, arise from operators that violate the lepton number by two units ($\Delta L=\pm2$) and conserve the baryon number ($\Delta B=0$). It was recently proven in Ref. [23], and considered earlier in Refs. [17,24], that operators in the SM with $|\Delta B-\Delta L|=2$ must have odd mass dimension. The operators included in our analysis are listed in Tables I (dimension five), II (dimension seven), and III (dimension nine). We consider operators with $d\leq9$ that contain neither (covariant) derivatives nor field strength tensors; the number of operators with $|\Delta L|=2$ grows quickly when $d\geq11$ (see Refs. [9,11,15]). Fields whose $SU(2)_L$ indices are contracted to form singlets are enclosed in parentheses; operators with the same field content but with different $SU(2)_L$ structures are listed separately. An operator may have multiple possible contractions of its $SU(3)_c$ and Lorentz indices. However, these different contractions lead to very similar estimates—they differ by at most $\mathcal{O}(1)$—for the amplitudes of LNV processes of interest here and will henceforth be ignored. A simple, concrete example is discussed in the Appendix.

As already mentioned in the Introduction, the effective operator approach employed here is complementary to the analyses in Ref. [19], in which a different set of effective operators is used. Specifically, the operators of Ref. [19] are constructed to be invariant under the low-energy symmetry group $SU(3)_c\times U(1)_{\rm EM}$ as opposed to the full SM gauge group. Figure 4 of that paper, for example, depicts experimental limits and sensitivities for the Wilson coefficient of the operator

$$(\bar{d}\gamma^\mu P_L u)(\bar{d}\gamma_\mu P_L u)(\overline{e^c}P_L\ell),\ \ell=e,\mu. \tag{3.1}$$

TABLE II. Same as Table I, for the dimension-seven operators featured in this analysis. Naming convention follows from Refs. [11,15].

$\mathcal{O}$	Operator	Λ [TeV]	$T_{0\nu\beta\beta}$ $R_{\mu^-e^+}$
$\mathcal{O}_2$	$(LL)(LH)e^c$	$4\times10^{6-7}$	$\ln(2)(\frac{\sqrt{2}}{G_F})^4(q^2)^2(\frac{16\pi^2}{y_\tau v^2})^2\frac{\Lambda^2}{Q^{11}}\sim10^{25}$–$10^{27}$ yr $(\frac{G_F}{\sqrt{2}})^2(\frac{1}{q^2})^2(\frac{y_\tau v^2}{16\pi^2})^2\frac{Q^6}{\Lambda^2}\sim10^{-38}$–$10^{-36}$
$\mathcal{O}_{3_a}$	$(LL)(QH)d^c$	$2\times10^{4-5}$	$\ln(2)(\frac{\sqrt{2}}{G_F})^2q^2\frac{\Lambda^2}{Q^{11}}[(\frac{G_F}{\sqrt{2}})^2\frac{1}{q^2}(\frac{y_bq^2v^2}{(16\pi^2)^2})^2+\frac{v^2}{\Lambda^4}]^{-1}\sim10^{24}$–$10^{26}$ yr $\frac{1}{q^2}\frac{Q^6}{\Lambda^6}[(\frac{G_F}{\sqrt{2}})^2\frac{1}{q^2}(\frac{y_bq^2v^2}{(16\pi^2)^2})^2+\frac{v^2}{\Lambda^4}]\sim10^{-37}$–$10^{-36}$
$\mathcal{O}_{3_b}$	$(LQ)(LH)d^c$	$1\times10^{7-8}$	$\ln(2)(\frac{\sqrt{2}}{G_F})^2q^2\frac{\Lambda^2}{Q^{11}}[(\frac{G_F}{\sqrt{2}})^2\frac{1}{q^2}(\frac{y_bv^2}{16\pi^2})^2+\frac{v^2}{\Lambda^4}]^{-1}\sim10^{25}$–$10^{27}$ yr $\frac{1}{q^2}\frac{Q^6}{\Lambda^2}[(\frac{G_F}{\sqrt{2}})^2\frac{1}{q^2}(\frac{y_bv^2}{16\pi^2})^2+\frac{v^2}{\Lambda^4}]\sim10^{-38}$–$10^{-36}$
$\mathcal{O}_{4_a}$	$(L\bar{Q})(LH)\overline{u^c}$	$4\times10^{8-9}$	$\ln(2)(\frac{\sqrt{2}}{G_F})^2q^2\frac{\Lambda^2}{Q^{11}}[(\frac{G_F}{\sqrt{2}})^2\frac{1}{q^2}(\frac{y_tv^2}{16\pi^2})^2+\frac{v^2}{\Lambda^4}]^{-1}\sim10^{25}$–$10^{27}$ yr $\frac{1}{q^2}\frac{Q^6}{\Lambda^2}[(\frac{G_F}{\sqrt{2}})^2\frac{1}{q^2}(\frac{y_tv^2}{16\pi^2})^2+\frac{v^2}{\Lambda^4}]\sim10^{-38}$–$10^{-36}$
$\mathcal{O}_{4_b}$	$(LL)(\bar{Q}H)\overline{u^c}$	2–7	This operator cannot contribute to $0\nu\beta\beta$. $\frac{v^2Q^6}{q^2\Lambda^2}[(\frac{G_F}{\sqrt{2}})^2(\frac{y_d}{g^2})^2(\frac{y_t}{16\pi^2})^2+\frac{1}{\Lambda^4}]\sim10^{-27}$–$10^{-24}$
$\mathcal{O}_8$	$(LH)\overline{e^c}\,\overline{u^c}\,d^c$	$6\times10^{2-3}$	$\ln(2)(\frac{\sqrt{2}}{G_F})^2q^2\frac{\Lambda^2}{Q^{11}}[(\frac{G_F}{\sqrt{2}})^2\frac{1}{q^2}(\frac{y_ty_bv}{(16\pi^2)^2})^2+\frac{v^2}{\Lambda^4}]^{-1}\sim10^{27}$–$10^{29}$ yr $\frac{1}{q^2}\frac{Q^6}{\Lambda^2}[(\frac{G_F}{\sqrt{2}})^2\frac{1}{q^2}(\frac{y_ty_by_\mu v^2}{(16\pi^2)^2})^2+\frac{v^2}{\Lambda^4}]\sim10^{-40}$–$10^{-38}$

TABLE III. Same as Table I, for the dimension-nine operators featured in this analysis. Naming convention follows from Refs. [11,15], with the exception of the singlet operator $\mathcal{O}_s$ [17].

$\mathcal{O}$	Operator	Λ [TeV]	$T_{0\nu\beta\beta}$ $R_{\mu^- e^+}$
$\mathcal{O}_5$	$(L\bar{H})(LH)(QH)d^c$	$6\times10^{4-5}$	$\ln(2)(\frac{\sqrt{2}}{G_F})^2 q^2 \frac{\Lambda^2}{Q^{11}}[(\frac{G_F}{\sqrt{2}})^2 \frac{1}{q^2}(\frac{y_b v^2}{(16\pi^2)^2})^2 + (\frac{v}{16\pi^2\Lambda^2}+\frac{v^3}{\Lambda^4})^2]^{-1} \sim 10^{25}$–$10^{27}$ yr $\frac{1}{q}\frac{Q^6}{\Lambda^2}[(\frac{G_F}{\sqrt{2}})^2 \frac{1}{q^2}(\frac{y_b v^2}{(16\pi^2)^2})^2 + (\frac{v}{16\pi^2\Lambda^2}+\frac{v^3}{\Lambda^4})^2] \sim 10^{-40}$–$10^{-38}$
$\mathcal{O}_6$	$(LH)(L\bar{H})(\bar{Q}H)\overline{u^c}$	$2\times10^{6-7}$	$\ln(2)(\frac{\sqrt{2}}{G_F})^2 q^2 \frac{\Lambda^2}{Q^{11}}[(\frac{G_F}{\sqrt{2}})^2 \frac{1}{q^2}(\frac{y_t v^2}{(16\pi^2)^2})^2 + (\frac{v}{16\pi^2\Lambda^2}+\frac{v^3}{\Lambda^4})^2]^{-1} \sim 10^{25}$–$10^{27}$ yr $\frac{1}{q}\frac{Q^6}{\Lambda^2}[(\frac{G_F}{\sqrt{2}})^2 \frac{1}{q^2}(\frac{y_t v^2}{(16\pi^2)^2})^2 + (\frac{v}{16\pi^2\Lambda^2}+\frac{v^3}{\Lambda^4})^2] \sim 10^{-37}$–$10^{-35}$
$\mathcal{O}_7$	$(LH)(QH)(\bar{Q}H)\overline{e^c}$	$4\times10^{1-2}$	$\ln(2)(\frac{\sqrt{2}}{G_F})^2 q^2 \frac{\Lambda^2}{Q^{11}}[(\frac{G_F}{\sqrt{2}})\frac{v}{(16\pi^2)^2}+\frac{v}{16\pi^2\Lambda^2}+\frac{v^3}{\Lambda^4}]^{-2} \sim 10^{22}$–$10^{24}$ yr $\frac{1}{q^2}\frac{Q^6}{\Lambda^2}[(\frac{G_F}{\sqrt{2}})\frac{v}{(16\pi^2)^2}+\frac{v}{16\pi^2\Lambda^2}+\frac{v^3}{\Lambda^4}]^2 \sim 10^{-34}$–$10^{-32}$
$\mathcal{O}_9$	$(LL)(LL)e^c e^c$	$3\times10^{2-3}$	$\ln(2)(\frac{\sqrt{2}}{G_F})^4 q^4 (\frac{16\pi^2}{y_\tau v})^4 \frac{\Lambda^2}{Q^{11}} \sim 10^{25}$–$10^{27}$ yr $(\frac{G_F}{\sqrt{2}})^2 \frac{1}{q^4}(\frac{y_\tau v}{16\pi^2})^4 \frac{Q^6}{\Lambda^2} \sim 10^{-38}$–$10^{-36}$
$\mathcal{O}_{10}$	$(LL)(LQ)e^c d^c$	$6\times10^{2-3}$	$\ln(2)(\frac{\sqrt{2}}{G_F})^2 q^2 \frac{\Lambda^2}{Q^{11}}[(\frac{G_F}{\sqrt{2}})^2 \frac{1}{q^2}(\frac{y_\tau y_b v^2}{(16\pi^2)^2})^2 + (\frac{y_\tau v}{16\pi^2\Lambda^2})^2]^{-1} \sim 10^{25}$–$10^{27}$ yr $\frac{1}{q^2}\frac{Q^6}{\Lambda^2}[(\frac{G_F}{\sqrt{2}})^2 \frac{1}{q^2}(\frac{y_\tau y_b v^2}{(16\pi^2)^2})^2 + (\frac{y_\tau v}{16\pi^2\Lambda^2})^2] \sim 10^{-38}$–$10^{-36}$
$\mathcal{O}_{11_a}$	$(LL)(QQ)d^c d^c$	3–30	$\ln(2)(\frac{\sqrt{2}}{G_F})^2 q^2 \frac{\Lambda^2}{Q^{11}}[(\frac{G_F}{\sqrt{2}})^2 \frac{1}{q^2}(\frac{y_b^2 g^2 v^2}{(16\pi^2)^3})^2 + (\frac{y_b v}{16\pi^2\Lambda^2})^2]^{-1} \sim 10^{22}$–$10^{26}$ yr $\frac{1}{q^2}\frac{Q^6}{\Lambda^2}[(\frac{G_F}{\sqrt{2}})^2 \frac{1}{q^2}(\frac{y_b^2 g^2 v^2}{(16\pi^2)^3})^2 + (\frac{y_b v}{16\pi^2\Lambda^2})^2] \sim 10^{-37}$–$10^{-33}$
$\mathcal{O}_{11_b}$	$(LQ)(LQ)d^c d^c$	$2\times10^{3-4}$	$\ln(2)\frac{\Lambda^2}{Q^{11}}[(\frac{G_F}{\sqrt{2}})^4 \frac{1}{q^4}(\frac{y_b^2 v^2}{(16\pi^2)^2})^2 + (\frac{G_F}{\sqrt{2}})^2 \frac{1}{q^2}(\frac{y_b v}{16\pi^2\Lambda^2})^2 + \frac{1}{\Lambda^8}]^{-1} \sim 10^{25}-10^{27}$ yr $\frac{Q^6}{\Lambda^2}[(\frac{G_F}{\sqrt{2}})^2 \frac{1}{q^4}(\frac{y_b^2 v^2}{(16\pi^2)^2})^2 + \frac{1}{q^2}(\frac{y_b v}{16\pi^2\Lambda^2})^2 + (\frac{\sqrt{2}}{G_F})^2 \frac{1}{\Lambda^8}] \sim 10^{-38}$–$10^{-36}$
$\mathcal{O}_{12_a}$	$(L\bar{Q})(L\bar{Q})\overline{u^c}\,\overline{u^c}$	$2\times10^{6-7}$	$\ln(2)\frac{\Lambda^2}{Q^{11}}[(\frac{G_F}{\sqrt{2}})^4 \frac{1}{q^4}(\frac{y_t^2 v^2}{(16\pi^2)^2})^2 + (\frac{G_F}{\sqrt{2}})^2 \frac{1}{q^2}(\frac{y_t v}{16\pi^2\Lambda^2})^2 + \frac{1}{\Lambda^8}]^{-1} \sim 10^{25}$–$10^{27}$ yr $\frac{Q^6}{\Lambda^2}[(\frac{G_F}{\sqrt{2}})^2 \frac{1}{q^4}(\frac{y_t^2 v^2}{(16\pi^2)^2})^2 + \frac{1}{q^2}(\frac{y_t v}{16\pi^2\Lambda^2})^2 + (\frac{\sqrt{2}}{G_F})^2 \frac{1}{\Lambda^8}] \sim 10^{-38}$–$10^{-36}$
$\mathcal{O}_{12_b}$	$(LL)(\bar{Q}\,\bar{Q})\overline{u^c}\,\overline{u^c}$	0.3–0.6	This operator cannot contribute to $0\nu\beta\beta$. $\frac{1}{q^2}\frac{Q^6}{\Lambda^2}[(\frac{G_F}{\sqrt{2}})^2(\frac{v y_\tau^2 y_d}{(16\pi^2)^2 g^2})^2 + (\frac{v y_t}{16\pi^2})^2 \frac{1}{\Lambda^4}] \sim 10^{-25}$–$10^{-23}$
$\mathcal{O}_{13}$	$(L\bar{Q})(LL)\overline{u^c}e^c$	$2\times10^{4-5}$	$\ln(2)(\frac{\sqrt{2}}{G_F})^2 q^2 \frac{\Lambda^2}{Q^{11}}[(\frac{G_F}{\sqrt{2}})^2 \frac{1}{q^2}(\frac{y_\tau y_t v^2}{(16\pi^2)^2})^2 + (\frac{y_\tau v}{16\pi^2\Lambda^2})^2]^{-1} \sim 10^{25}$–$10^{27}$ yr $\frac{1}{q^2}\frac{Q^6}{\Lambda^2}[(\frac{G_F}{\sqrt{2}})^2 \frac{1}{q^2}(\frac{y_\tau y_t v^2}{(16\pi^2)^2})^2 + (\frac{y_\tau v}{16\pi^2\Lambda^2})^2] \sim 10^{-37}$–$10^{-35}$
$\mathcal{O}_{14_a}$	$(LL)(Q\bar{Q})\overline{u^c}d^c$	10^{2-3}	$\ln(2)(\frac{\sqrt{2}}{G_F})^2 q^2 \frac{\Lambda^2}{Q^{11}}[(\frac{G_F}{\sqrt{2}})^2 \frac{1}{q^2}(\frac{y_t y_b g^2 v^2}{(16\pi^2)^3})^2 + (\frac{y_t v}{16\pi^2\Lambda^2})^2]^{-1} \sim 10^{24}$–$10^{26}$ yr $\frac{1}{q^2}\frac{Q^6}{\Lambda^2}[(\frac{G_F}{\sqrt{2}})^2 \frac{1}{q^2}(\frac{y_t y_b g^2 v^2}{(16\pi^2)^3})^2 + (\frac{y_t v}{16\pi^2\Lambda^2})^2] \sim 10^{-37}$–$10^{-35}$
$\mathcal{O}_{14_b}$	$(L\bar{Q})(LQ)\overline{u^c}d^c$	$6\times10^{4-5}$	$\ln(2)\frac{\Lambda^2}{Q^{11}}[(\frac{G_F}{\sqrt{2}})^4 \frac{1}{q^4}(\frac{y_t y_b v^2}{(16\pi^2)^2})^2 + (\frac{G_F}{\sqrt{2}})^2 \frac{1}{q^2}(\frac{y_t v}{16\pi^2\Lambda^2})^2 + \frac{1}{\Lambda^8}]^{-1} \sim 10^{25}$–$10^{27}$ yr $\frac{Q^6}{\Lambda^2}[(\frac{G_F}{\sqrt{2}})^2 \frac{1}{q^4}(\frac{y_t y_b v^2}{(16\pi^2)^2})^2 + \frac{1}{q^2}(\frac{y_t v}{16\pi^2\Lambda^2})^2 + (\frac{\sqrt{2}}{G_F})^2 \frac{1}{\Lambda^8}] \sim 10^{-38}$–$10^{-36}$
$\mathcal{O}_{15}$	$(LL)(L\bar{L})d^c\overline{u^c}$	10^{2-3}	$\ln(2)(\frac{\sqrt{2}}{G_F})^4 \frac{\Lambda^2}{Q^{11}}[\frac{1}{q^2}(\frac{y_t y_b g^2 v^2}{(16\pi^2)^3}) + (\frac{y_t y_b v^2}{(16\pi^2)^2\Lambda^4})]^{-2} \sim 10^{24}$–$10^{26}$ yr $(\frac{G_F}{\sqrt{2}})^2 \frac{Q^6}{\Lambda^2}[\frac{1}{q^2}(\frac{y_t y_b g^2 v^2}{(16\pi^2)^3}) + (\frac{y_t y_b v^2}{(16\pi^2)^2\Lambda^4})]^2 \sim 10^{-37}$–$10^{-35}$
$\mathcal{O}_{16}$	$(LL)e^c d^c\overline{e^c}\,\overline{u^c}$	0.2–2	$\ln(2)(\frac{\sqrt{2}}{G_F})^2 q^2 \frac{\Lambda^2}{Q^{11}}[(\frac{G_F}{\sqrt{2}})^2 \frac{1}{q^2}(\frac{y_t y_b g^4 v^2}{(16\pi^2)^4})^2 + (\frac{y_\tau v}{16\pi^2\Lambda^2})^2]^{-1} \sim 10^{16}$–$10^{22}$ yr $\frac{1}{q^2}\frac{Q^6}{\Lambda^2}[(\frac{G_F}{\sqrt{2}})^2 \frac{1}{q^2}(\frac{y_t y_b g^4 v^2}{(16\pi^2)^4})^2 + (\frac{y_\tau v}{16\pi^2\Lambda^2})^2] \sim 10^{-33}$–$10^{-27}$
$\mathcal{O}_{17}$	$(LL)d^c d^c\overline{d^c}\,\overline{u^c}$	0.2–2	$\ln(2)(\frac{\sqrt{2}}{G_F})^2 q^2 \frac{\Lambda^2}{Q^{11}}[(\frac{G_F}{\sqrt{2}})^2 \frac{1}{q^2}(\frac{y_t y_b g^4 v^2}{(16\pi^2)^4})^2 + (\frac{q g^2}{(16\pi^2)^2\Lambda^2})^2]^{-1} \sim 10^{23}$–$10^{26}$ yr $\frac{1}{q^2}\frac{Q^6}{\Lambda^2}[(\frac{G_F}{\sqrt{2}})^2 \frac{1}{q^2}(\frac{y_t y_b g^4 v^2}{(16\pi^2)^4})^2 + (\frac{q g^2}{(16\pi^2)^2\Lambda^2})^2] \sim 10^{-37}$–$10^{-34}$

(Table continued)

TABLE III. *(Continued)*

$\mathcal{O}_{18}$	$(LL)d^c u^c \overline{u^c}\,\overline{u^c}$	0.2–2	$\ln(2)(\frac{\sqrt{2}}{G_F})^2 q^2 \frac{\Lambda^2}{Q^{11}}[(\frac{G_F}{\sqrt{2}})^2 \frac{1}{q^2}(\frac{y_t y_b g^4 v^2}{(16\pi^2)^3})^2 + (\frac{q q^2}{(16\pi^2)^2\Lambda^2})^2]^{-1} \sim 10^{23}$–$10^{26}$ yr $\frac{1}{q^2}\frac{Q^6}{\Lambda^2}[(\frac{G_F}{\sqrt{2}})^2 \frac{1}{q^2}(\frac{y_t y_b g^4 v^2}{(16\pi^2)^3})^2 + (\frac{q q^2}{(16\pi^2)^2\Lambda^2})^2] \sim 10^{-37}$–$10^{-34}$
$\mathcal{O}_{19}$	$(LQ)d^c d^c \overline{e^c}\,\overline{u^c}$	0.1–1	$\ln(2)\frac{\Lambda^2}{Q^{11}}[(\frac{G_F}{\sqrt{2}})^4 \frac{1}{q^4}(\frac{y_t y_t^2 y_e v^2}{(16\pi^2)^3})^2 + (\frac{G_F}{\sqrt{2}})^2 \frac{1}{q^2}(\frac{y_b v}{16\pi^2\Lambda^2})^2 + \frac{1}{\Lambda^8}]^{-1} \sim 10^{10}$–$10^{19}$ yr $\frac{Q^6}{\Lambda^2}[(\frac{G_F}{\sqrt{2}})^2 \frac{1}{q^4}(\frac{y_t y_b^2 y_\mu v^2}{(16\pi^2)^3})^2 + \frac{1}{q^2}(\frac{y_b v}{16\pi^2\Lambda^2})^2 + (\frac{\sqrt{2}}{G_F})^2 \frac{1}{\Lambda^8}] \sim 10^{-30}$–$10^{-21}$
$\mathcal{O}_{20}$	$(L\bar{Q})d^c \overline{u^c}\,\overline{e^c}\,\overline{u^c}$	4–40	$\ln(2)\frac{\Lambda^2}{Q^{11}}[(\frac{G_F}{\sqrt{2}})^4 \frac{1}{q^4}(\frac{y_t^2 y_b y_e v^2}{(16\pi^2)^3})^2 + (\frac{G_F}{\sqrt{2}})^2 \frac{1}{q^2}(\frac{y_t v}{16\pi^2\Lambda^2})^2 + \frac{1}{\Lambda^8}]^{-1} \sim 10^{19}$–$10^{25}$ yr $\frac{Q^6}{\Lambda^2}[(\frac{G_F}{\sqrt{2}})^2 \frac{1}{q^4}(\frac{y_t^2 y_b y_\mu v^2}{(16\pi^2)^3})^2 + \frac{1}{q^2}(\frac{y_t v}{16\pi^2\Lambda^2})^2 + (\frac{\sqrt{2}}{G_F})^2 \frac{1}{\Lambda^8}] \sim 10^{-35}$–$10^{-30}$
$\mathcal{O}_s$	$e^c e^c u^c u^c \overline{d^c}\,\overline{d^c}$	10^{-3}	$\ln(2)\frac{\Lambda^2}{Q^{11}}[(\frac{G_F}{\sqrt{2}})^4 \frac{1}{q^4}(\frac{y_t^2 y_b^2 y_e^2 v^2}{(16\pi^2)^4})^2 + (\frac{G_F}{\sqrt{2}})^2 \frac{1}{q^2}(\frac{y_t y_b y_e v}{(16\pi^2)^2\Lambda^2})^2 + \frac{1}{\Lambda^8}]^{-1} \sim 10^{-20}$–$10^{-10}$ yr $\frac{Q^6}{\Lambda^2}[(\frac{G_F}{\sqrt{2}})^2 \frac{1}{q^4}(\frac{y_t^2 y_b^2 y_\mu^2 v^2}{(16\pi^2)^4})^2 + \frac{1}{q^2}(\frac{y_t y_b y_\mu v}{(16\pi^2)^2\Lambda^2})^2 + (\frac{\sqrt{2}}{G_F})^2 \frac{1}{\Lambda^8}] \sim 10^{-1}$–$10^{9}$

This low-energy operator is descended from the following SM-gauge-invariant operators:

$$\mathcal{O}_{47_a} = (L\overline{Q})(L\overline{Q})(HQ)(HQ), \tag{3.2}$$

$$\mathcal{O}_{47_d} = L\bar{Q})(LQ)(HQ)(H\bar{Q}), \tag{3.3}$$

where we have used the naming convention of Refs. [11,15]. These operators have mass-dimension 11, and thus lie outside the scope of this work.

In the absence of neutrino masses, the SM exhibits global $U(1)$ symmetries associated with each lepton flavor, electron number, muon number, and tau number. This is no longer the case in the presence of beyond-the-standard-model physics, and lepton-flavor numbers are necessarily violated if the global lepton number is violated. The operators in Tables I, II, and III can distribute their lepton-number violations among the lepton families. For instance, the Weinberg operator $\mathcal{O}_1$ should be generalized to

$$\frac{1}{\Lambda}(LH)(LH) \to \frac{1}{\Lambda}[f_{ee}(L_eH)(L_eH) + f_{e\mu}(L_eH)(L_\mu H) + f_{e\tau}(L_eH)(L_\tau H) + \cdots], \tag{3.4}$$

where $L_\alpha, \alpha = e, \mu, \tau$ are the electron-flavor, muon-flavor, or tau-flavor lepton doublets; Λ is the effective energy scale of the operator; and the coefficients $f_{\alpha\beta} = f_{\beta\alpha}$, $\alpha, \beta = e, \mu, \tau$, characterize the operator's distinct flavor components. We define Λ such that the largest $f_{\alpha\beta}$ is unity. The amplitude for $0\nu\beta\beta$ is proportional to f_{ee}, and the amplitude for the $\mu^- \to e^+$ conversion is proportional to $f_{e\mu}$. The series in Eq. (3.4) also produces rare LNV decays such as $K^+ \to \pi^-\mu^+\mu^+$ and $\tau^- \to \mu^+\pi^-\pi^-$, as well as lepton-number violation at collider experiments. The limits on $f_{\alpha\beta}/\Lambda$ from these processes are not competitive with limits from $0\nu\beta\beta$ and $\mu^- \to e^+$ conversion for the relevant lepton-flavor structure, and we do not consider them here.[1] The $f_{\alpha\beta}$ do not mix with one another via renormalization-group running due to SM interactions, because lepton-flavor numbers are conserved in the SM.[2] We describe the relative strengths of the independent lepton-flavor components of $d \geq 7$ operators via coefficients $g_{\alpha\beta\gamma\cdots}$, $\alpha, \beta, \gamma, \ldots = e, \mu, \tau$. These are the analogues of $f_{\alpha\beta}$ in Eq. (3.4). In this work, we assume, for simplicity, that the high-scale physics may distinguish between different lepton flavors but treats quark flavors democratically, so we suppress quark-flavor indices.

The operators listed in Tables I, II, and III can also be related to Majorana neutrino masses, as discussed in Refs. [9,11,15].[3] In a nutshell, the idea is to postulate that UV physics explicitly violates the lepton number and that, at the tree level, it manifests itself predominantly as one of the $d \geq 7$ operators listed in Tables I, II, and III. At the loop level, SM interactions imply that the same physics will lead to nonzero neutrino masses via the Weinberg operator $\mathcal{O}_1$. Hence, these tree-level operators induce operators of lower mass dimension. Their coefficients can be related by closing external legs into loops and inserting SM interactions. This procedure implies that $f_{\alpha\beta}$ are linear combinations of the $g_{\alpha\beta\cdots}$.

After electroweak symmetry is broken, the neutrino masses are proportional to the eigenvalues of the matrix $f_{\alpha\beta}$, and the leptonic mixing matrix U is the matrix of its eigenvectors. In Refs. [11,15], the contributions of these operators to the Weinberg operator are estimated using a

[1]Recent, detailed discussions and estimates can be found, for instance, in Refs. [18,25–29].

[2]We are ignoring the possibility for neutrino Yukawa couplings, which could give rise to lepton-flavor violation at low energies.

[3]The singlet operator $\mathcal{O}_s$ is included in neither of these analyses because one requires very small $\Lambda \sim \mathcal{O}(\text{GeV})$ in order to explain the observed neutrino masses. It is, however, discussed briefly in Ref. [17].

procedure similar to the one we outline in Sec. IV. A range for Λ is determined based on the criterion that the largest entries in the neutrino mass matrix lie within $m_\nu \in 0.05$–0.5 eV, with higher Λ corresponding to lower m_ν. The third column of Tables I, II, and III lists these ranges of Λ.

Operators $\mathcal{O}_{4_b}$ in Table II and $\mathcal{O}_{12_b}$ in Table III require extra care. These operators are necessarily antisymmetric in the flavors of the two lepton doublets. In addition to the antisymmetry of their weak indices, the Lorentz structure of these operators requires contraction between the lepton doublets, leaving only the flavor indices to enforce the overall antisymmetry. This feature had been overlooked in previous estimates of the contributions of these operators to the neutrino mass matrix. The simplest diagrams one can write down to generate a Majorana neutrino mass for $\mathcal{O}_{4_b}$ ($\mathcal{O}_{12_b}$) are a pair of two-loop (three-loop) diagrams that sum to zero due to this antisymmetry; this is similar to what one encounters in calculating the contributions of neutrino magnetic moment operators to the neutrino mass matrix, as in Ref. [30]. Following Ref. [30], the leading contributions to the neutrino mass matrix come from inserting two Yukawa interactions into these diagrams to form either the dimension-seven equivalent of the Weinberg operator or the dimension-five Weinberg operator $\mathcal{O}_1$ at one additional loop level. We update the estimates for the contributions of these operators to the neutrino matrix in Ref. [11] as follows:

$$\mathcal{O}_{4_b}\colon\ m_{\alpha\beta} = g_{\alpha\beta}\left(\frac{1}{16\pi^2}+\frac{v^2}{\Lambda^2}\right)\frac{y_t g^2 (y_\beta^2 - y_\alpha^2)}{(16\pi^2)^2}\frac{v^2}{\Lambda}, \tag{3.5}$$

$$\mathcal{O}_{12_b}\colon\ m_{\alpha\beta} = g_{\alpha\beta}\left(\frac{1}{16\pi^2}+\frac{v^2}{\Lambda^2}\right)\frac{y_t^2 g^2 (y_\beta^2 - y_\alpha^2)}{(16\pi^2)^3}\frac{v^2}{\Lambda}, \tag{3.6}$$

where y_t is the top-quark Yukawa coupling; y_α is the Yukawa coupling for charged lepton $\alpha = e, \mu, \tau$; g is the weak coupling constant; and v is the Higgs vacuum expectation value. Because $g_{\alpha\beta}$ is antisymmetric, these matrices have vanishing diagonal elements: $m_{ee} = m_{\mu\mu} = m_{\tau\tau} = 0$. We recalculate the values of Λ for each operator such that the largest element of the mass matrix lies within $m_\nu \in 0.05$–0.5 eV; the results are listed in Tables II and III.

It is not possible, in a model-independent way, to relate LNV processes mediated by the new physics, e.g., $0\nu\beta\beta$ and $\mu^- \to e^+$ conversion, because the different $g_{\alpha\beta\ldots}$ are not related. Majorana neutrino masses, however, serve as a link between otherwise disconnected LNV phenomena. If the neutrino masses and the leptonic mixing matrix were known, it would be possible, assuming the physics responsible for nonzero neutrino masses was captured by one of the operators in Tables I, II, and III, to translate constraints on LNV processes—such as those mentioned below Eq. (3.4)—into constraints on other LNV processes. An important consequence of the connection between Majorana neutrino masses and LNV phenomena is that the observation of any LNV decay, interaction, etc., implies that neutrinos have a Majorana component to their masses, and that the existence of a Majorana neutrino mass implies that some LNV phenomena occur [31]. Exactly which processes must occur, however, cannot be predicted *a priori*.

Even partial information on neutrino masses and lepton mixing allows one to relate different LNV phenomena. As an example, we discuss the connection between Majorana neutrino masses and LNV phenomena using $0\nu\beta\beta$ and the $\mu^- \to e^+$ conversion assuming the Weinberg operator $\mathcal{O}_1$ captures the bulk of LNV phenomena. If neutrino exchange dominates these processes—the case of $\mathcal{O}_1$—the rate of $0\nu\beta\beta$ is proportional to

$$|m_{ee}|^2 \equiv |U_{e1}^2 m_1 + U_{e2}^2 m_2 e^{i\alpha_1} + U_{e3}^2 m_3 e^{i\alpha_2}|^2, \tag{3.7}$$

while the rate of the $\mu^- \to e^+$ conversion is proportional to

$$|m_{e\mu}|^2 \equiv |U_{e1}U_{\mu 1} m_1 + U_{e2}U_{\mu 2} m_2 e^{i\alpha_1} + U_{e3}U_{\mu 3} m_3 e^{i\alpha_2}|^2, \tag{3.8}$$

where m_i is the mass of ν_i, $U_{\alpha i}$ are the elements of the leptonic mixing matrix U, and α_i are potential Majorana phases. If nothing were known about the neutrino masses and mixing parameters, nothing could be said about m_{ee} in relation to $m_{e\mu}$. However, from current measurements of the leptonic mixing matrix and the neutrino mass-squared differences [32], we find that m_{ee} and $m_{e\mu}$ can only vanish simultaneously for very specific values of the unknown m_1, α_1, and α_2 parameters. This implies that if LNV manifests itself predominantly via $\mathcal{O}_1$, modulo special circumstances that are probably related to a special symmetry, at least one of $0\nu\beta\beta$ and $\mu^- \to e^+$ conversion must occur.

Neutrino exchange does not, however, always dominate the amplitudes for these processes, as we discuss in detail in Sec. IV. Even so, we have verified, for all operators in Tables I, II, and III, that if m_{ee} ($m_{e\mu}$) is nonzero the amplitude for $0\nu\beta\beta$ ($\mu^- \to e^+$ conversion) does not vanish as long as the dominant LNV physics is captured by one of the operators in Tables I, II, and III. There is no guarantee, of course, that the nonzero rate is within experimental reach. If more operators are present with commensurate strength, we cannot rule out the possibility of fortuitous cancellations.

IV. ESTIMATES AND COMPARISONS

In this section, we describe the process used for estimating $0\nu\beta\beta$ half-lives ($T_{0\nu\beta\beta}$) and $\mu^- \to e^+$ conversion rates ($R_{\mu^- e^+}$), concentrating, for concreteness, on $\mathcal{O}_{14_b}$. In Sec. IV A, we discuss $0\nu\beta\beta$, and in Sec. IV B we discuss the $\mu^- \to e^+$ conversion in nuclei. We estimate the values of

diagrams with incoming (outgoing) down quarks and outgoing (incoming) up quarks for $0\nu\beta\beta$ ($\mu^- \to e^+$ conversion), and we bypass effects from hadronic currents, nuclear matrix elements, phase-space integration, etc., In order to make comparisons with existing and future experimental results, we take advantage of existing bounds on [33] or calculations of [34,35] the light neutrino exchange contribution, as will become clear momentarily.

A. Neutrinoless double beta decay

Here, we discuss how we estimate $T_{0\nu\beta\beta}$ for the operator $\mathcal{O}_{14_b} = (L\overline{Q})(LQ)\overline{u^c}d^c$. We separate the discussion into contributions at tree level, one loop, and two loops. We reemphasize that these are rough estimates aimed at capturing the dominant contributing factors to $0\nu\beta\beta$ and comparing these different contributions. Much more thorough calculations involving hadronic currents, etc., are necessary in order to extract accurate bounds. For our purposes, however, order-of-magnitude estimates are sufficient.

1. Tree level

Figure 1(a) depicts the dominant tree-level contribution from $\mathcal{O}_{14_a}$ for $0\nu\beta\beta$. The amplitude scales as Λ^{-5} since $\mathcal{O}_{14_a}$ has mass dimension nine. We use the variable Q, which has dimensions of mass and encodes all information related to phase-space, nuclear matrix elements, etc., in order to convert the diagram into a decay rate, via naive dimensional analysis. Q is naively of order the Q value of the decay process, a few MeV. Our estimate is

$$\Gamma^{(0)}_{0\nu\beta\beta} = |g_{ee}|^2 \frac{Q^{11}}{\Lambda^{10}}, \tag{4.1}$$

where g_{ee} reflects the fact that this contribution requires both of the lepton doublets to be of electron flavor.

2. One loop

Here we consider the diagram shown in Fig. 1(b). When calculating a loop contribution, we assume the momentum cutoff scale to be Λ, above which the effective field theory approach is no longer valid. Each loop also contributes a factor of $(16\pi^2)^{-1}$ to the amplitude. We estimate the contribution of this loop to the amplitude to be

$$\int \frac{d^4p}{(2\pi)^4 p^2} \sim \frac{\Lambda^2}{16\pi^2}. \tag{4.2}$$

The amplitude, therefore, scales as Λ^{-3}. The Higgs boson can be replaced by its vacuum expectation value v which multiplies its coupling to the up-type quark in the loop. We choose to take all effective operators to be quark-flavor universal, so the largest contribution to this diagram comes from the top quark, proportional to y_t, the top quark Yukawa coupling. The W-boson propagator and couplings contribute a factor of $G_F/\sqrt{2}$. The dominant contribution from the neutrino propagator scales like $1/q^2$, which we estimate is of order $(100\ \mathrm{MeV})^{-2}$, the typical distance scale between nucleons. Therefore, we estimate

$$\Gamma^{(1)}_{0\nu\beta\beta} = |g_{ee}|^2 \left(\frac{G_F}{\sqrt{2}}\right)^2 \left(\frac{1}{q^2}\right) \left(\frac{v y_t}{16\pi^2}\right)^2 \frac{Q^{11}}{\Lambda^6}. \tag{4.3}$$

Since the neutrino propagator is not exactly pointlike, the phase-space-matrix-element-etc.,-Q^2 factor here is not identical to the one in Eq. (4.1). The difference—not more than an order of magnitude—is too small to impact our results and will be ignored.

3. Two loop

The dominant contribution at two-loop order comes from the diagram shown in Fig. 1(c). Here, one loop contributes the same factor discussed above, and the second contributes

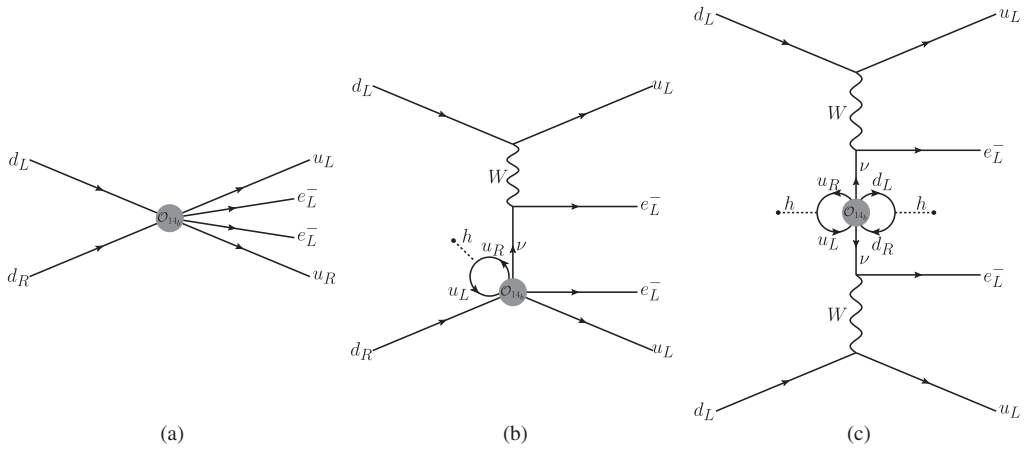

FIG. 1. Feynman diagrams contributing to $0\nu\beta\beta$ from the operator $\mathcal{O}_{14_b} = (L\overline{Q})(LQ)\overline{u^c}d^c$. The dominant contributions scaling as (a) $\Gamma \sim \Lambda^{-10}$, (b) Λ^{-6}, and (c) Λ^{-2} are depicted.

the same factor but with the bottom quark Yukawa coupling y_b instead of the top quark Yukawa coupling y_t. Additionally, there are two W-boson propagators instead of one. The neutrino propagator contributes a factor proportional to $1/q^2$ on top of the mass-insertion associated with the two-loop diagram. The estimate, therefore, is

$$\Gamma^{(2)}_{0\nu\beta\beta} = |g_{ee}|^2 \left(\frac{G_F}{\sqrt{2}}\right)^4 \left(\frac{1}{q^2}\right)^2 \left(\frac{y_t y_b v^2}{(16\pi^2)^2}\right)^2 \frac{Q^{11}}{\Lambda^2} = \left(\frac{G_F}{\sqrt{2}}\right)^4 \left(\frac{1}{q^2}\right)^2 |m_{ee}|^2 Q^{11}. \quad (4.4)$$

This diagram is exactly the neutrino exchange process discussed in Sec. III; hence we have rewritten the width as proportional to $|m_{ee}|^2$. For $\mathcal{O}_{14_b}$, the neutrino mass matrix in the flavor basis is estimated to be

$$m_{\alpha\beta} = \frac{g_{\alpha\beta}}{\Lambda} \frac{y_t y_b v^2}{(16\pi^2)^2}, \quad (4.5)$$

$\alpha, \beta = e, \mu, \tau$. As in the case of Eq. (4.3), the phase-space-matrix-element-etc.,-Q^2 factor here is not identical to the one in Eq. (4.1), but the difference can, given our goals, be safely ignored.

We use the results from the KamLAND-Zen experiment, along with the upper bound they compute for $|m_{ee}|$, in order to extract the value of Q^{11} by requiring that Eq. (4.4) exactly reproduces the KamLAND-Zen result; i.e., we obtain the lower bound on the half-life for the quoted upper bound on $|m_{ee}|$. Concretely, the bound $T_{0\nu\beta\beta} > 1.07 \times 10^{26}$ (90% C.L.) from KamLAND-Zen, which can be translated into $m_{ee} < 100$ meV—here we make a concrete choice about the relevant nuclear matrix element—results into $Q = 11$ MeV.

For most values of Λ, the total decay rate is dominated by $\Gamma^{(0)}_{0\nu\beta\beta}$, $\Gamma^{(1)}_{0\nu\beta\beta}$, or $\Gamma^{(2)}_{0\nu\beta\beta}$. For certain values of Λ, however, the different amplitudes are of the same order of magnitude, and one should also take interference effects into account. For $\mathcal{O}_{14_b}$, the tree-level, one-loop, and two-loop processes would add incoherently if the quarks were massless and were not bound to nucleons and nuclei, since they involve different chiral quark fields (see Fig. 1). Our procedure for estimating the different contributions does not, however, allow us to evaluate the sign or the magnitude of these interference effects. We address this shortfall by considering the cases where interference between the different diagrams is as constructive as possible or as destructive as possible. Figure 2 depicts the half-life $T_{0\nu\beta\beta} = \log(2)/\Gamma_{0\nu\beta\beta}$ as a function of Λ assuming either perfectly constructive (lower curve) or perfectly destructive interference among the different contributions. Also shown are the current bound on $T_{0\nu\beta\beta} > 1.07 \times 10^{26}$ yr (90% C.L.) from the KamLAND-Zen experiment [33] along with the range of Λ where $\mathcal{O}_{14_b}$ leads to neutrino masses between 0.05 and 0.5 eV, as listed in Table III. In the case of perfect destructive interference, the lifetime estimates satisfy the current upper bounds for a very narrow range of values of Λ around 70 GeV and 1 TeV. Outside of these narrow ranges, or if perfect destructive interference is not present, interference effects do not significantly impact order-of-magnitude estimates of the decay rate. If we assume $|g_{ee}|^2 = 1$ and that $\mathcal{O}_{14_b}$ is responsible for neutrino masses, we estimate $T_{0\nu\beta\beta} \sim 10^{25} - 10^{27}$ yr. On the other hand, absent very strong interference effects and assuming $|g_{ee}|^2 = 1$, the current bounds on $T_{0\nu\beta\beta}$ translates into $\Lambda \gtrsim 10^5$ TeV. The current upper bound on $T_{0\nu\beta\beta}$ implies that the dominant contribution to $0\nu\beta\beta$ coming from UV physics that manifests itself at the tree level as $\mathcal{O}_{14_b}$ comes from massive neutrino exchange.

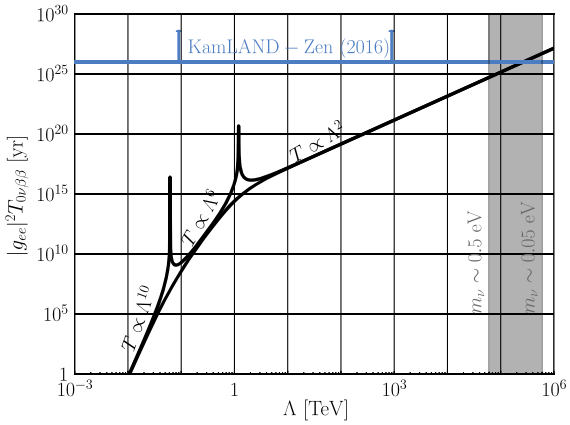

FIG. 2. The $0\nu\beta\beta$ half-life $T_{0\nu\beta\beta}$ as a function of the scale of new physics Λ for operator $\mathcal{O}_{14_b}$. The pink line displays the current bound (assuming $|g_{ee}|^2 = 1$) by the KamLAND-Zen experiment [33], $T_{0\nu\beta\beta} > 1.07 \times 10^{26}$ yr (90% C.L.), and the grey region shows the range of Λ necessary to generate neutrino masses between 0.05 and 0.5 eV. Three distinct regions are visible on the graph, where $T \propto \Lambda^{10}$, Λ^6, and Λ^2. These regions correspond to when the diagrams in Figs. 1(a), 1(b), and 1(c) are dominant in this process, respectively.

B. $\mu^- \to e^+$ conversion

In order to estimate the rate of $\mu^- \to e^+$ conversion, we first address the muon capture rate. As this is a weak-interaction process, it is proportional to the probability density function of the incoming muon $|\psi_{100}(0)|^2$ (which we assume to be in the 1s ground state of the atom), so we estimate

$$\Gamma(\mu\text{capture}) \sim \left(\frac{G_F}{\sqrt{2}}\right)^2 Q^2 \left(\frac{Z^3_{\text{eff}}}{\pi(a_0 m_e/m_\mu)^3)}\right), \quad (4.6)$$

where a_0 is the Bohr radius and Q is a number with dimensions of mass that contains information regarding

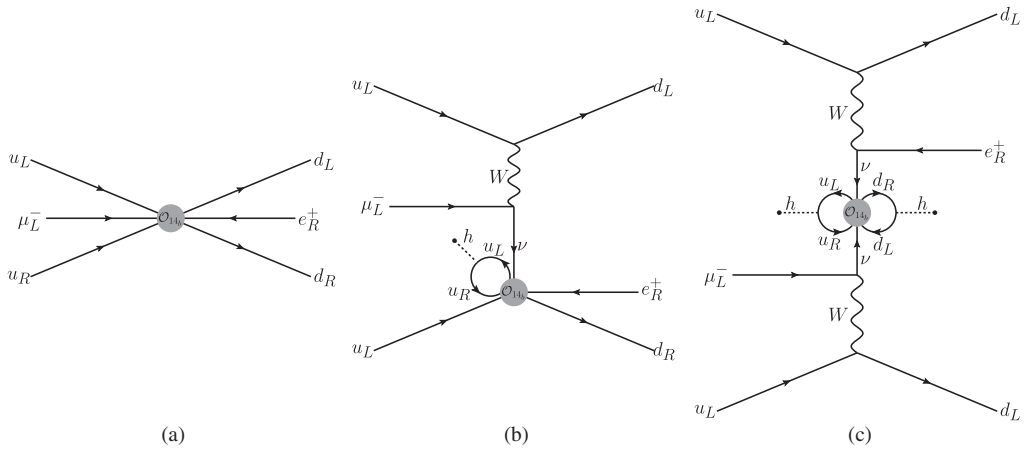

FIG. 3. Feynman diagrams contributing to $\mu^- \to e^+$ conversion from the operator $\mathcal{O}_{14_b} = (L\bar{Q})(LQ)\overline{u^c}d^c$. The dominant contributions scaling as (a) $\Gamma \sim \Lambda^{-10}$, (b) Λ^{-6}, and (c) Λ^{-2} are shown.

phase space, nuclear matrix elements, etc., similar to the equivalent variable in the $0\nu\beta\beta$-decay discussion. Note that, here, the Q value of the reaction is of order the muon mass. The last factor in parentheses is $|\psi_{100}(0)|^2$. The rate for $\mu^- \to e^+$ conversion depends on $|\psi_{100}(0)|^2$ as well, which cancels out in estimating $R_{\mu^-e^+}$.

Figure 3 shows the dominant diagrams contributing at (a) tree level, (b) one loop, and (c) two loops to $\mu^- \to e^+$ conversion. These are very similar to Figs. 1(a), 1(b), and 1(c), respectively. The contributions to $R_{\mu^-e^+}$ from Figs. 3(a), 3(b), and 3(c) can be estimated following the same steps that led to Eqs. (4.1), (4.3), and (4.4), respectively. We find

$$R^{(0)}_{\mu^-e^+} = |g_{e\mu}|^2 \left(\frac{\sqrt{2}}{G_F}\right)^2 \frac{Q^6}{\Lambda^{10}}, \tag{4.7}$$

$$R^{(1)}_{\mu^-e^+} = |g_{e\mu}|^2 \left(\frac{1}{q^2}\right) \left(\frac{y_t v}{16\pi^2}\right)^2 \frac{Q^6}{\Lambda^6}, \tag{4.8}$$

$$R^{(2)}_{\mu^-e^+} = |g_{e\mu}|^2 \left(\frac{G_F}{\sqrt{2}}\right)^2 \left(\frac{1}{q^2}\right)^2 \left(\frac{y_t y_b v^2}{(16\pi^2)^2}\right)^2 \frac{Q^6}{\Lambda^2}. \tag{4.9}$$

Similar to Eq. (4.4), Eq. (4.9) can be written as a coefficient times $|m_{e\mu}|^2$; see Eq. (4.5). As in Sec. IV A, the Q^2 factors are not strictly the same for the tree-level, one-loop, and two-loop contributions, but we assume that differences are sufficiently small and can be safely ignored.

References [34,35] estimated $R_{\mu^-e^+}$ for light neutrino exchange,

$$R_{\mu^-e^+} = (2.6 \times 10^{-22}) |\mathcal{M}_{e\mu^+}|^2 \frac{|m_{e\mu}|^2}{m_e^2}, \tag{4.10}$$

where m_e is the electron mass and $|\mathcal{M}_{e\mu^+}|$ is the nuclear matrix element, estimated to lie, for titanium, between 0.03 and 0.5. Similar to what we did in Sec. IV A, we solve for Q in the estimates above so that Eq. (4.9) matches the more precise estimate, Eq. (4.10), for $|\mathcal{M}_{e\mu^+}| = 0.1$, which we assume is the value of the nuclear matrix element for aluminum to sodium transition. Setting all nuclear matrix elements the same for different transitions is only a simplifying assumption that may be violated by more sophisticated estimates.

As with $0\nu\beta\beta$ interference effects—which cannot be reliably evaluated following the procedure outlined here—need to be considered when the contributions of the different amplitudes are of the same order of magnitude. Figure 4 depicts the normalized conversion rate $R_{\mu^-e^+}$ as a

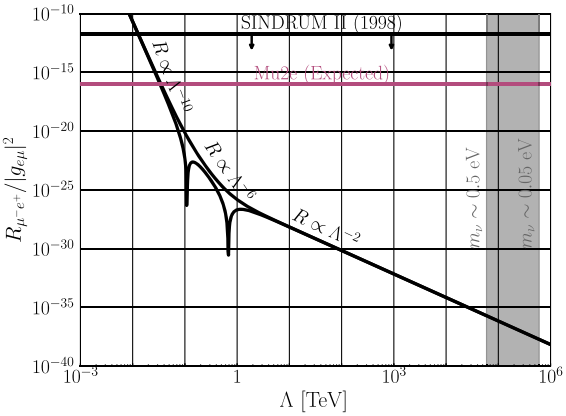

FIG. 4. The $\mu^- \to e^+$ conversion rate $R_{\mu^-e^+}$ as a function of the scale of new physics Λ for operator $\mathcal{O}_{14_b}$. The black line displays the current bound by the SINDRUM II Collaboration, while the blue line indicates our estimate of the reach of the Mu2e experiment, both assuming $|g_{e\mu}|^2 = 1$. The grey region highlights the range of Λ necessary to generate neutrino masses between 0.05 and 0.5 eV. Three distinct regions are visible on the graph, where $T \propto \Lambda^{10}$, Λ^6, and Λ^2. These regions correspond to when the diagrams in Figs. 1(a), 1(b), and 1(c) are dominant in this process, respectively.

TABLE IV. Constants used for estimating $T_{0\nu\beta\beta}$ and $R_{\mu^-e^+}$. The Q value for $0\nu\beta\beta$ refers to the isotope ^{136}Xe, and the Q value for $\mu^- \to e^+$ refers to the isotope ^{27}Al.

Constant	G_F [GeV^{-2}]	g	$\langle r \rangle$	v [GeV]	Q [MeV]	y_t	y_b	y_e	y_μ	y_τ
Value	1.17×10^{-5}	0.653	(100 MeV)$^{-1}$	174	11.0 ($0\nu\beta\beta$), 15.6 ($\mu^- \to e^+$)	0.9	2×10^{-2}	3×10^{-6}	6×10^{-4}	10^{-2}

function of Λ assuming either perfect constructive interference (upper curve) or perfect destructive interference (lower curve). Also shown is the range of Λ where $\mathcal{O}_{14_b}$ leads to neutrino masses between 0.05 and 0.5 eV, as listed in Table III. If we assume that $\mathcal{O}_{14_b}$ is responsible for neutrino masses, $\Lambda \sim 6 \times 10^{4-5}$ TeV, and we estimate that $R_{\mu^-e^+} \simeq 10^{-38} - 10^{-36}$, further assuming $|g_{e\mu}|^2 = 1$. The current bound on $R_{\mu^-e^+} < 1.7 \times 10^{-12}$ from the SINDRUM II Collaboration, again assuming $|g_{e\mu}|^2 = 1$, implies $\Lambda \gtrsim 10$ GeV. As discussed in Sec. II, we expect the Mu2e experiment will be sensitive to $R_{\mu^-e^+} \gtrsim 10^{-16}$ and is hence expected to observe $\mu^- \to e^+$ conversion if $\Lambda \lesssim 40$ GeV.

V. RESULTS

We follow the steps outlined for $\mathcal{O}_{14_b}$ in Sec. IV and estimate the rates for $0\nu\beta\beta$ and $\mu^- \to e^+$ conversion for all effective operators listed in Tables I, II, and III. Analytic results are listed in Tables I, II, and III. The results for $0\nu\beta\beta$ agree with the estimates presented in Ref. [11], while the $\mu^- \to e^+$ conversion rates are the main results of this paper.

In order to convert analytic expressions into numerical estimates for observables or the sensitivity to the new physics scale Λ, we use the values listed in Table IV for various SM parameters. y_f denotes the Yukawa coupling of fermion f, g denotes the weak gauge coupling, and v denotes the vacuum expectation value of the Higgs field. The variables Q—different for $R_{\mu^-e^+}$ and $T_{0\nu\beta\beta}$—were defined in Sec. IV and are used to map our very rough estimates to more precise computations of $R_{\mu^-e^+}$ and $T_{0\nu\beta\beta}$. We further assume that the operator coefficients $g_{\alpha\beta\ldots}$ are all $\mathcal{O}(1)$. As discussed in Sec. III, this is not necessarily the case and should be kept under advisement. Several operators, e.g., $\mathcal{O}_{13}$, contain four or more leptons, and the resulting $0\nu\beta\beta$ and $\mu^- \to e^+$ amplitudes depend on a weighted sum of coefficients $g_{\alpha\beta\gamma\delta}$, typically of the form $\sum_\gamma g_{\alpha\beta\gamma\gamma} y_{l_\gamma}$, where y_{l_γ} is the Yukawa coupling of the lepton of flavor γ. In these instances, we assume that $g_{\alpha\beta ee} \sim g_{\alpha\beta\mu\mu} \sim g_{\alpha\beta\tau\tau}$ and list only the largest contribution, usually due to the latter thanks to the relatively large tau Yukawa coupling. Numerical estimates for all observables under investigation are also listed in Tables I, II, and III, assuming the operator in question is responsible for the observable neutrino masses; i.e., the value of Λ agrees with the associated tabulated values of Λ. All estimates here, and the expressions tabulated in the tables, are obtained assuming that amplitudes that involve different chiral incoming and outgoing fermion fields do not interfere. This is a good approximation for most values of Λ except for a few narrow ranges and only if it turns out that interference effects are strongly destructive, as discussed in Sec. IV. We have verified that the results associated with the $\mu^- \to e^+$ conversion turn out not to be significantly impacted by interference effects. Perfect destructive interference—if present—could weaken the bounds associated with $0\nu\beta\beta$ for most of the effective operators discussed here, except for $\mathcal{O}_{1,2,8,9,11_a,16,17,18,s}$. We do not allow for this possibility here.

Figures 5, 6, and 7 depict the currently allowed values of Λ assuming current and future experimental bounds for operators of mass-dimension five, seven, and nine, respectively. For each operator, we depict the estimated bound for Λ using the bound on $R_{\mu^-e^+}$ from SINDRUM II (black), the estimated sensitivity of Mu2e (pink), and the estimated bound on Λ using the results on $T_{0\nu\beta\beta}$ from the KamLAND-ZEN experiment (blue). All estimates are valid for $g_{\alpha\beta\ldots} = \mathcal{O}(1)$. A hierarchical structure among the flavor coefficients could impair the ability to place a bound on Λ from $0\nu\beta\beta$ or $\mu^- \to e^+$ conversion, for instance. Also shown for each operator is the range of Λ such that $m_{\alpha\beta} \simeq 0.05$–$0.5$ eV.

As before, we direct the reader's attention to $\mathcal{O}_{4_b}$ and $\mathcal{O}_{12_b}$. These operators must have vanishing g_{ee} due to the flavor antisymmetry of the lepton doublets, meaning neither of these operators can produce $0\nu\beta\beta$, as indicated

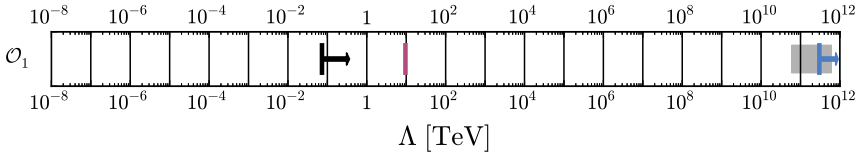

FIG. 5. Bounds on the effective scale associated with the dimension-five operator $\mathcal{O}_1$ from the KamLAND-Zen experiment for $0\nu\beta\beta$ (blue) and SINDRUM-II experiment for $\mu^- \to e^+$ (black). Also shown are the estimated sensitivity for the Mu2e experiment (pink) and the range of Λ for which $m_{\alpha\beta} \sim 0.05$–$0.5$ eV (grey). We assume $g_{\alpha\beta\ldots} = 1$ for all coefficients here. See text for details.

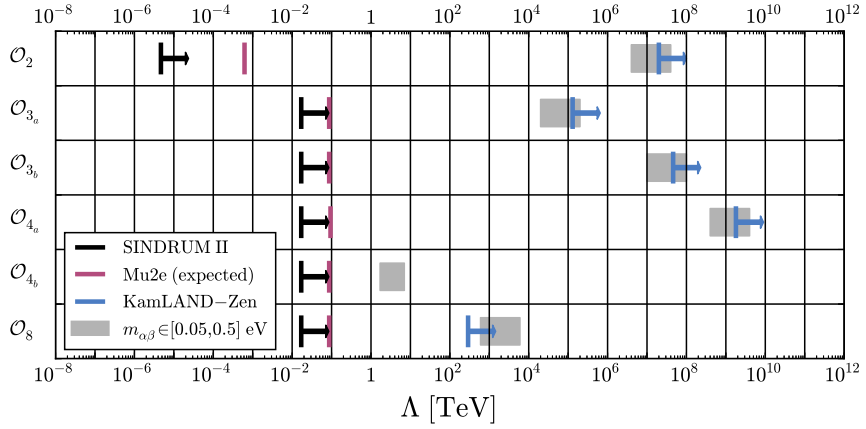

FIG. 6. Bounds on the effective scale associated with the dimension-seven operators $\mathcal{O}_{2,3_a,3_b,4_a,4_b,8}$ from the KamLAND-Zen experiment for $0\nu\beta\beta$ (blue) and SINDRUM-II experiment for $\mu^- \to e^+$ (black). Also shown are the estimated sensitivity of the Mu2e experiment (pink) and the range of Λ for which $m_{\alpha\beta} \sim 0.05$–$0.5$ eV (grey). We assume $g_{\alpha\beta\ldots} = 1$ for all coefficients here. See text for details.

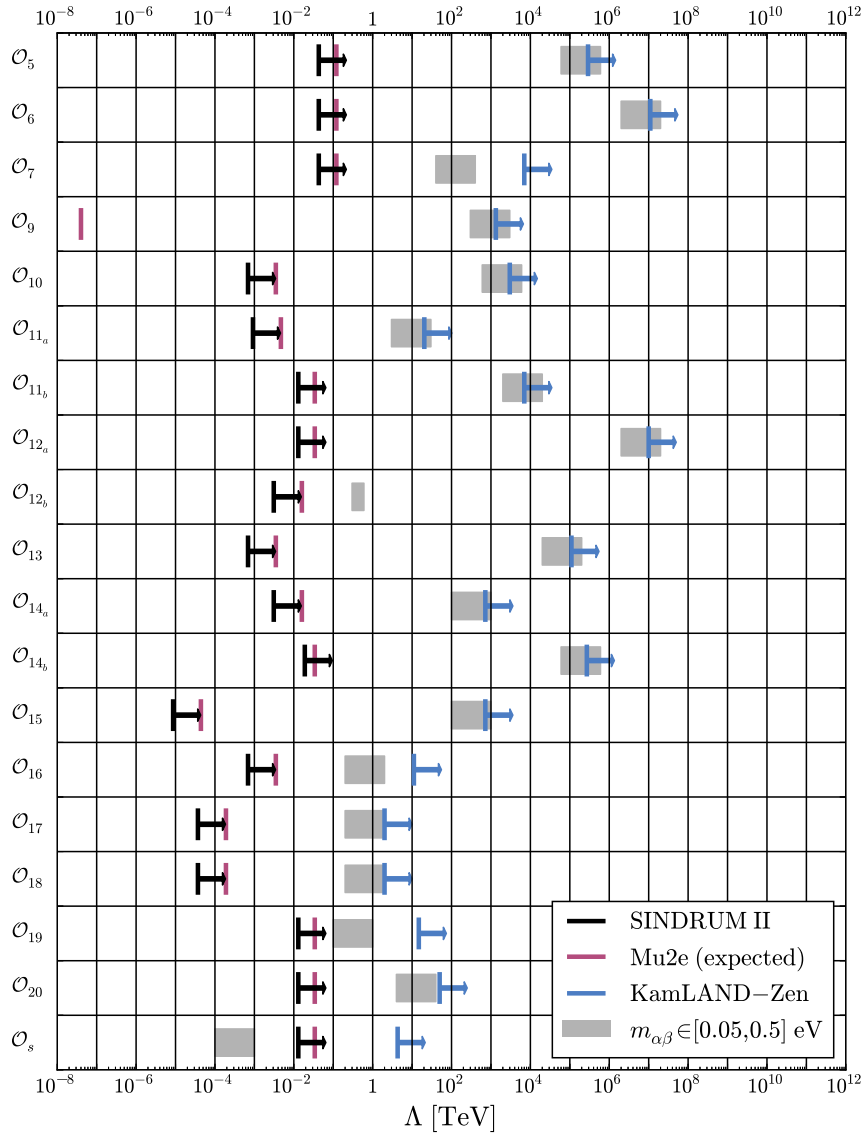

FIG. 7. Bounds on the effective scale associated with the dimension-nine operators listed in Table III from the KamLAND-Zen experiment for $0\nu\beta\beta$ (blue) and SINDRUM-II experiment for $\mu^- \to e^+$ (black). Also shown are the estimated sensitivity of the Mu2e experiment (pink) and the range of Λ for which $m_{\alpha\beta} \sim 0.05$–$0.5$ eV (grey). We assume $g_{\alpha\beta\ldots} = 1$ for all coefficients here. See text for details.

in Tables II and III. There is no such restriction on $g_{e\mu}$. This means that, in principle, $\mu^- \to e^+$ conversion could occur at an observable rate in next-generation experiments in the complete absence of $0\nu\beta\beta$ if either of these operators were the only source of lepton-number violation. We note, however, that the neutrino mass matrices in Eqs. (3.5) and (3.6) have vanishing diagonal elements, resulting in a mass matrix with relatively few independent degrees of freedom. This produces strong correlations among the neutrino masses and leptonic mixing parameters, such that current neutrino oscillation data preclude either of these operators from being the dominant contribution to neutrino masses and mixings (see, for instance, Refs. [36–38]).

VI. DISCUSSION AND CONCLUSIONS

The observation of LNV phenomena would imply that the neutrinos are Majorana fermions and would help point the community to a subset of ideas for the new physics behind nonzero neutrino masses. The absence of LNV phenomena would not necessarily allow one to conclude that neutrinos are Dirac fermions, but a prolonged absence, assuming many different probes, would lead one to ultimately suspect this is the case and would point the search for the origin of nonzero neutrino masses down a very different path. Hence, deep and broad searches for the validity of lepton-number conservation are among the highest priorities of experimental particle physics today.

Here, we concentrated on understanding the reach of searches for $\mu^- \to e^+$ conversion in nuclei, partially motivated by the fact that, in the foreseeable future, several new experiments are aiming at improving the sensitivity to $\mu^- \to e^-$ conversion by 4 or more orders of magnitude. We opted for an effective operator approach that allows one to compare a large number of new physics scenarios.

At face value, future searches for $\mu^- \to e^+$ conversion are sensitive to new, LNV physics at a wide range of effective energy scales, from 100 MeV to 10 TeV.[4] This sensitivity pales in comparison with searches for $0\nu\beta\beta$, as revealed in Figs. 5, 6, and 7. Comparisons between different LNV observables, however, need to be interpreted with care. Flavor effects can, as is well known, render the rate for $0\nu\beta\beta$ infinitesimally small and need not impact different LNV observables in the same way.

LNV new physics ultimately leads to nonzero neutrino masses. Figures 5, 6, and 7 also reveal that if the dominant contribution to the neutrino masses is captured individually by any of the effective operators discussed here, the expected rates for $\mu^- \to e^+$ conversion are well beyond the reach of next generation experiments, with one trivial exception.[5] All of these observations imply that, should the $\mu^- \to e^+$ conversion be discovered in the next round of experiments, we will be able to conclude that (i) neutrinos are Majorana fermions; (ii) flavor effects, or something equivalent, significantly suppress the rate for $0\nu\beta\beta$; and (iii) the physics behind nonzero neutrino masses, assuming all new degrees of freedom are heavy, does not manifest itself at tree level via one of the effective operators investigated here but, instead, is captured by a nontrivial combination of operators whose contributions to the Majorana neutrino masses are significantly smaller than the contributions of any one operator.

ACKNOWLEDGMENTS

We thank Alex Merle for valuable feedback. A. d. G. thanks Bob Bernstein for conversations and discussions that inspired some of this work. A. K. thanks Bill Molzon for useful conversations and feedback. The work of J. M. B., A. d. G., and K. J. K. is supported in part by DOE Grant No. DE-SC0010143. The work of A. K. is supported in part by DOE Grant No. DE-SC0009919.

Note added.—After this work was completed, Ref. [39] appeared on the preprint archive. In it, the authors present a detailed calculation of the rate of the $\mu^- \to e^+$ conversion for a model with a doubly charged scalar, as well as a discussion of how to map specific models of new physics onto effective operator coefficients.

APPENDIX: EXPLICIT NEW PHYSICS SCENARIO

Here we outline an ultraviolet-complete scenario of new physics in order to illustrate how the effective operators of Tables I, II, and III might arise, as well as to illustrate the procedure for estimating the contributions of such operators to the LNV phenomena of interest.

Concretely, we add two scalar fields, ρ and Φ, to the SM particle content. Their charges under the SM gauge group are

$$\rho \sim (\mathbf{3},\mathbf{1})_{-1/3}, \qquad \Phi = \begin{pmatrix} \varphi_1 \\ \varphi_2 \end{pmatrix} \sim (\mathbf{3},\mathbf{2})_{1/6}, \tag{A1}$$

where the notation indicates in parentheses the $SU(3)_c$ and $SU(2)_L$ representations, followed by the hypercharges.

[4]Except for $\mathcal{O}_9$. For $\Lambda \gtrsim 1$ GeV, the effective operator approaches are still valid for the $\mu^- \to e^+$ conversion in nuclei, as long as the new physics is not very weakly coupled. It is, however, difficult to imagine that, for $\Lambda \lesssim 100$ GeV, the existence of these new degrees of freedom is not severely constrained by probes of new phenomena that do not involve lepton-number violation. The exploration of such constraints cannot, however, be pursued within the formalism adopted here.

[5]If $\mathcal{O}_s$ was responsible for nonzero neutrino masses, its effective scale would be around 1 GeV, and either $0\nu\beta\beta$ decay or $\mu^- \to e^+$ conversion should have been observed a long time ago, along with many more non-LNV observables.

In addition to the standard kinetic and mass terms for ρ and Φ, the symmetries of the SM allow for the following interactions:

$$\Delta\mathcal{L} = -\mu\rho(\Phi^\dagger H) - \lambda_1^\alpha \rho^\dagger (L_\alpha Q) - \lambda_2^\beta (\Phi L_\beta) d^c - \kappa^\alpha \rho e_\alpha^c u^c + \text{H.c.}, \tag{A2}$$

where, as before, parentheses denote fields whose $SU(2)_L$ indices have been contracted, and α, β are lepton-flavor indices; all other indices have been suppressed. We continue to assume that the new physics is independent of quark flavor.

Integrating out ρ and Φ using Eq. (A2) induces a tree-level contribution to the operator $\mathcal{O}_{3b}$. Explicitly,

$$\mathcal{O}_{3b} = \frac{g_{\alpha\beta}}{\Lambda^3}(L^\alpha Q)(L^\beta H) d^c, \tag{A3}$$

where

$$\frac{g_{\alpha\beta}}{\Lambda^3} = \frac{\lambda_1^\alpha \lambda_2^\beta \mu}{M^4}. \tag{A4}$$

Here M are the masses of ρ and Φ, which we assume are identical for simplicity. Choosing the largest $g_{\alpha\beta} = 1$, as discussed in the text, Eq. (A4) is the definition of the effective scale Λ associated with the effective operator $\mathcal{O}_{3b}$ while $g_{\alpha\beta} \propto \lambda_1^\alpha \lambda_2^\beta$. If $\mu \sim M$—which one may argue is a reasonable criterion, from the point of view of naturalness—then $\Lambda \sim M$ if λ_1, $\lambda_2 \sim 1$. As is well known, if, for example, the new physics is very weakly coupled (λ_1, $\lambda_2 \ll 1$), the masses of the new degrees of freedom are much lighter than the effective scale of the operator that describes the low-energy consequences of the new physics.

At low energies, integrating out ρ and Φ also leads to $\mathcal{O}_8$, its coefficient proportional to $\kappa^\alpha \lambda_2^\beta$. However, assuming $\lambda_1^\alpha \sim \kappa^\alpha$, the contributions of $\mathcal{O}_{3_b}$ to LNV phenomena overwhelm those from $\mathcal{O}_8$—see Table II. For this reason, we restrict our remaining discussions to $\kappa^\alpha = 0$, for simplicity and clarity.

Figure 8(a) depicts the tree-level contribution to $0\nu\beta\beta$ within this model, and Fig. 8(b) depicts the one-loop contribution. While the contribution from Fig. 8(a) is already captured by Eq. (A4), after integrating out the heavy scalars (note that we refer to φ_2 in the diagram, as we are interested in the broken phase), we must execute a loop integral in order to determine the contribution of Fig. 8(b). This contribution is finite and, assuming a vanishing down-quark mass, is given by

$$\lambda_1^e \lambda_2^e \int \frac{d^4p}{(2\pi)^4} \frac{\mu \times \not{p}\not{p}}{(p^2 - M^2)^2 \cdot p^2 \cdot p^2} = \frac{(-i)\lambda_1^e \lambda_2^e \mu}{(4\pi)^2 M^2} \mathbb{1} \sim \frac{1}{\Lambda^3}\left(\frac{-i\Lambda^2}{16\pi^2}\right)\mathbb{1}, \tag{A5}$$

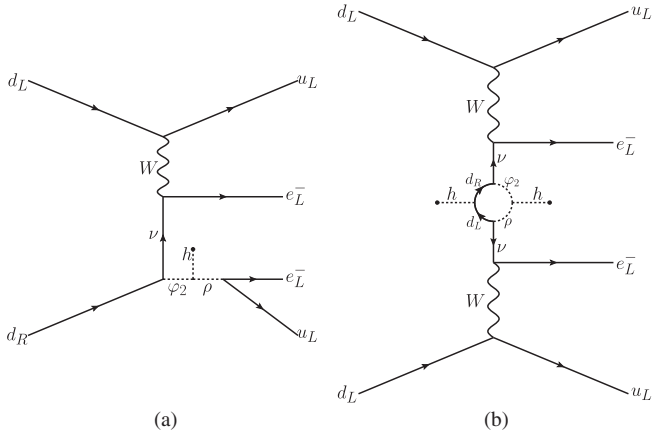

FIG. 8. (a) The tree-level and (b) one-loop-level contributions of $0\nu\beta\beta$ from the model presented in Eq. (A2).

where in the last step we assume $\mu \sim M \sim \Lambda$ and $\lambda_1^e, \lambda_2^e \sim 1$. The familiar factor $\Lambda^2/16\pi^2$ is directly related to the prescription described in Eq. (4.2). The one-loop part of the diagram Fig. 8(b) is, of course, the Weinberg operator. There are more detailed discussions of the validity of this prescription, including concrete examples, in Refs. [11,15].

An in-depth analysis of this model is well beyond the scope of this work; instead, we outline some simple phenomenological considerations. The potential of the new scalars must be such that neither acquires a vacuum expectation value, or else $SU(3)_c$ gauge invariance would be spontaneously broken. Moreover, they must be sufficiently heavy in order to elude searches for new heavy colored states at the Large Hadron Collider (LHC) and in order to bypass severe constraints from flavor observables.[6] From Table II, $\Lambda \gtrsim \mathcal{O}(10^7)$ TeV is required if the physics responsible for $\mathcal{O}_{3_b}$ is directly related to the observed neutrino masses. This means that, assuming $M \sim \Lambda$, the new degrees of freedom are heavy enough that collider or flavor constraints are easily satisfied.

It is easy to check that Eq. (A2) conserves the baryon number (both ρ and Φ can be assigned baryon number $+1/3$) so there are no constraints from proton decay or other baryon-number-violating phenomena. On the other hand, Eq. (A2) violates the lepton number—indeed, it was designed to do just that—but does so only if all three new-physics couplings λ_1, λ_2, and μ are nonzero. This implies that LNV observables are, necessarily, proportional to the product $\lambda_1\lambda_2\mu$ and that nonzero Majorana neutrino masses occur only at the one-loop level.

[6] ρ or Φ exchange potentially mediate, at the tree level, the $\mu^- \to e^-$ conversion in nuclei.

[1] A. de Gouvêa and P. Vogel, Lepton flavor and number conservation, and physics beyond the standard model, Prog. Part. Nucl. Phys. **71**, 75 (2013).

[2] W. Rodejohann, Neutrino-less double beta decay and particle physics, Int. J. Mod. Phys. E **20**, 1833 (2011).

[3] M. Lindner, M. Platscher, and F. S. Queiroz, A call for new physics: The muon anomalous magnetic moment and lepton flavor violation, arXiv:1610.06587.

[4] Y. G. Cui *et al.* (COMET Collaboration), Report No. KEK-2009-10 (2009).

[5] H. Natori (DeeMe Collaboration), DeeMe experiment—an experimental search for a mu-e conversion reaction at J-PARC MLF, Nucl. Phys. B, Proc. Suppl. **248–250**, 52 (2014).

[6] L. Bartoszek *et al.* (Mu2e Collaboration), Mu2e technical design report, arXiv:1501.05241.

[7] Y. Kuno, Rare lepton decays, Prog. Part. Nucl. Phys. **82**, 1 (2015).

[8] J. Kaulard *et al.* (SINDRUM II Collaboration), Improved limit on the branching ratio of $\mu^- \to e^+$ conversion on titanium, Phys. Lett. B **422**, 334 (1998).

[9] K. S. Babu and C. N. Leung, Classification of effective neutrino mass operators, Nucl. Phys. **B619**, 667 (2001).

[10] G. Prezeau, M. Ramsey-Musolf, and P. Vogel, Neutrinoless double beta decay and effective field theory, Phys. Rev. D **68**, 034016 (2003).

[11] A. de Gouvêa and J. Jenkins, Survey of lepton number violation via effective operators, Phys. Rev. D **77**, 013008 (2008).

[12] J. Bergstrom, A. Merle, and T. Ohlsson, Constraining new physics with a positive or negative signal of neutrino-less double beta decay, J. High Energy Phys. 05 (2011) 122.

[13] F. del Aguila, A. Aparici, S. Bhattacharya, A. Santamaria, and J. Wudka, Effective Lagrangian approach to neutrino-less double beta decay and neutrino masses, J. High Energy Phys. 06 (2012) 146.

[14] F. Bonnet, M. Hirsch, T. Ota, and W. Winter, Systematic decomposition of the neutrinoless double beta decay operator, J. High Energy Phys. 03 (2013) 055; Erratum, J. High Energy Phys. 04 (2014) 090.

[15] P. W. Angel, N. L. Rodd, and R. R. Volkas, Origin of neutrino masses at the LHC: $\Delta L = 2$ effective operators and their ultraviolet completions, Phys. Rev. D **87**, 073007 (2013).

[16] J. C. Helo, M. Hirsch, T. Ota, and F. A. Pereira dos Santos, Double beta decay and neutrino mass models, J. High Energy Phys. 05 (2015) 092.

[17] A. de Gouvêa, J. Herrero-Garcia, and A. Kobach, Neutrino masses, grand unification, and baryon number violation, Phys. Rev. D **90**, 016011 (2014).

[18] A. Atre, V. Barger, and T. Han, Upper bounds on lepton-number violating processes, Phys. Rev. D **71**, 113014 (2005).

[19] T. Geib, A. Merle, and K. Zuber, $\mu^- - e^+$ conversion in upcoming LFV experiments, Phys. Lett. B **764**, 157 (2017).

[20] W. H. Bertl *et al.* (SINDRUM II Collaboration), A search for muon to electron conversion in muonic gold, Eur. Phys. J. C **47**, 337 (2006).

[21] Y. Kuno, COMET and PRISM: Search for charged lepton flavor violation with muons, Nucl. Phys. B, Proc. Suppl. **225–227**, 228 (2012).

[22] C. Dohmen *et al.* (SINDRUM II Collaboration), Test of lepton flavor conservation in $\mu^- \to e^+$ conversion on titanium, Phys. Lett. B **317**, 631 (1993).

[23] A. Kobach, Baryon number, lepton number, and operator dimension in the standard model, Phys. Lett. B **758**, 455 (2016).

[24] S. Rao and R. E. Shrock, Six Fermion $(B - L)$ violating operators of arbitrary generational structure, Nucl. Phys. **B232**, 143 (1984).

[25] A. Atre, T. Han, S. Pascoli, and B. Zhang, The search for heavy Majorana neutrinos, J. High Energy Phys. 05 (2009) 030.

[26] J. Gluza and T. Jeliński, Heavy neutrinos and the $pp \to lljj$ CMS data, Phys. Lett. B **748**, 125 (2015).

[27] J. Gluza, T. Jeliński, and R. Szafron, Lepton number violation and "Diracness", of massive neutrinos composed of Majorana states, Phys. Rev. D **93**, 113017 (2016).

[28] T. Golling *et al.*, Physics at a 100 TeV pp collider: Beyond the standard model phenomena, arXiv:1606.00947.

[29] N. Quintero, Constraints on lepton number violating short-range interactions from $|\Delta L| = 2$ processes, Phys. Lett. B **764**, 60 (2017).

[30] N. F. Bell, M. Gorchtein, M. J. Ramsey-Musolf, P. Vogel, and P. Wang, Model independent bounds on magnetic moments of Majorana neutrinos, Phys. Lett. B **642**, 377 (2006).

[31] J. Schechter and J. W. F. Valle, Neutrino decay and spontaneous violation of lepton number, Phys. Rev. D **25**, 774 (1982).

[32] K. A. Olive *et al.* (Particle Data Group Collaboration), Review of particle physics, Chin. Phys. C **38**, 090001 (2014).

[33] A. Gando *et al.* (KamLAND-Zen Collaboration), Search for Majorana Neutrinos near the Inverted Mass Hierarchy Region with KamLAND-Zen, Phys. Rev. Lett. **117**, 082503 (2016); Erratum, Phys. Rev. Lett. **117**, 109903(E) (2016).

[34] F. Simkovic, P. Domin, S. V. Kovalenko, and A. Faessler, The (μ^-, e^+) conversion in nuclei mediated by light Majorana neutrinos, Part. Nucl. Lett. **104**, 40 (2001).

[35] P. Domin, S. Kovalenko, A. Faessler, and F. Simkovic, Nuclear (μ^-, e^+) conversion mediated by Majorana neutrinos, Phys. Rev. C **70**, 065501 (2004).

[36] P. H. Frampton, S. L. Glashow, and D. Marfatia, Zeroes of the neutrino mass matrix, Phys. Lett. B **536**, 79 (2002).

[37] Z.-z. Xing, in *Neutrino Oscillations and Their Origin: Proceedings of the 5th International Workshop, NOON2004, Tokyo, Japan, 2004* (World Scientific, Singapore, 2005), pp. 442–449.

[38] M. Singh, G. Ahuja, and M. Gupta, Revisiting the texture zero neutrino mass matrices, Prog. Theor. Exp. Phys. **2016**, 123B08 (2016).

[39] T. Geib and A. Merle, $\mu^- - e^+$ Conversion from short-range operators, Phys. Rev. D **95**, 055009 (2017).